R. Vescovini, C. Bisagni
Semi-Analytical Buckling Analysis of Omega Stiffened Panels Under Multi-Axial Loads
Composite Structures, Vol. 120, 2015, p. 285-299
doi:10.1016/j.compstruct.2014.10.003

Semi-Analytical Buckling Analysis of Omega Stiffened Panels under Multi-Axial Loads

Riccardo Vescovini*and Chiara Bisagni

Department of Aerospace Science and Technology, Politecnico di Milano

Via La Masa 34, 20156 Milano, Italy

Abstract

This paper presents a semi-analytical method for the buckling analysis of composite panels reinforced with omega stiffeners and subjected to combined loading conditions of biaxial loads and shear. The approach is based on the representation of the panel as an assembly of plate elements, allowing to capture local buckling modes involving skin and stiffener deflections. The panel model includes also the possibility of accounting for the stiffener foot. Trigonometric shape functions are introduced to describe the buckling patterns, while the buckling equations are derived through the application of the minimum potential energy principle. The comparison with Abaqus finite element analyses is presented, demonstrating, for a wide variety of test cases, percent differences below 9% and a good accuracy of the computed buckling modes. The computational speed up is of the order of 100, suggesting the use of the formulation in the context of preliminary design loops, sensitivity analyses or design optimizations.

Keywords: stiffened panels; buckling; semi-analytical methods; omega stiffeners.

1 Introduction

Composite stiffened panels are commonly used in load-bearing components of aerospace structures. As they usually operate under combined loads that can promote buckling phenomena, the ability to accurately predict the local buckling is an essential task since the preliminary design phases.

The most common approach to evaluate the buckling load is based on the finite element method [1, 2], whose advantages rely on the accuracy of the results, as well as the possibility of accounting for various boundary and loading conditions. However, a major drawback is represented by the time to perform the analyses, which can be inappropriate in the early design stages. Furthermore, geometric modeling is required, and finite element

*Corresponding author. *Tel:* +39 02 23998332, *email address:* riccardo.vescovini@polimi.it (Riccardo Vescovini)

meshes have to be created for each configurations under investigation.

The finite strip method is a numerical procedure specifically developed for the analysis of prismatic structures [3] and is characterized by an improved computational efficiency. The method has been successfully applied to assess the buckling behaviour of stiffened panels [4], to study the effects of different stiffener geometries [5], and to perform structural optimizations with buckling requirements [6].

An even more efficient approach consists in the use of ad-hoc developed analytical formulations. In this case, the buckling load is calculated in a reduced time, so that sensitivity studies and design optimizations can be easily performed [7–9]. In this case, the accuracy of the results can be strongly affected by several assumptions regarding the modeling of the panel, the loading conditions and the stacking sequences. Some formulations available in literature simplify the stiffened panels as isolated plates with simply-supported or clamped constraints along the skin edges. The introduction of this assumption allows to derive, in the case of compression loads, the expression for the buckling load in a closed-form manner. The solutions are available for panels of isotropic and orthotropic [10] materials, as well as symmetric [11] and unsymmetric [12] laminates. More complex loading conditions are usually handled with semi-analytical strategies. For instance, combined loads are studied by Chai and Hoon [13] for simply-supported panels, while linearly varying biaxial in-plane loads are accounted for in the formulation of Romeo and Frulla [14]. Similarly, Shufrin et al. [15] consider general in-plane conditions by applying the extended method of Kantorovich. The assumption of simply-supported or clamped edges does not account for the finite amount of restraint provided by the stiffeners and, for this reason, can be the source of inaccurate results. In some other studies, the stiffener is modeled as a torsion spring or a De Saint-Venant torsion bar. Even in this case, the closed-form solutions are generally limited to the case of compression loads. Closed-form solutions are derived for orthotropic panels also by Bisagni and Vescovini [16] and Mittelstedt and Beerhorst [17], representing the stiffeners as torsion bars and torsion springs, respectively. Biaxial compression, in-plane bending and shear loads are introduced in the semi-analytical formulation of Bedair [18] for isotropic panels partially restrained against rotation and in-plane translation. Wittenberg et al. [19] investigate the shear buckling of stiffened panels with orthotropic skin lay-up, considering the flexural and torsional stiffness of the stiffeners with a formulation based on the method of Galerkin. In general, the methods accounting for the restraint to the edge rotation guarantee more accurate buckling predictions in comparison to those based on the assumption of simply-supported and clamped conditions. However, they still furnish a simplified description of the interaction between the skin and the stiffener, and local stiffener buckling modes cannot be captured.

The methods where both the skin and the stiffeners are modeled as two-dimensional plate elements allow for a more accurate representation of the skin-stiffener interaction, and both skin and local stiffener instabilities can be accounted for. The formulation of Fujikubo and Yao [20] derive closed-form solutions for the buckling load of isotropic stiffened panels, using a plate assembly model and energy principles and considering compression loads only.

Semi-analytical strategies are developed by Byklum and Amdahl [21] and Buermann et al. [22] in the context of the large deflection analysis of J-stiffened panels. They consider multiaxial loading conditions of compression and shear loads for isotropic materials. Composite materials were considered by the authors [23] in a formulation where double sines functions were used to represent the out of plane displacements. In general, all the mentioned methods introduce the simplifying assumption of neglecting the foot of the stiffener, i.e. the flange connecting the stiffener to the skin.

The present work discusses a plate assembly model for the buckling analysis of composite omega stiffened panels. Compared to most of the other methods in literature, the formulation introduces the possibility of considering the presence of the foot of the stiffener. The spectrum of loading conditions and laminate lay-ups is extended to include biaxial tension/compression and shear. Flexural anisotropy is accounted for, so that a wide class of typical aeronautical laminates can be studied.

The formulation is based on the minimum potential energy principle, which is applied referring to the method of Ritz. The governing equations are derived analytically and the computation of the buckling load is reduced to the solution of a set of eigenproblems of small dimension. The design tool is applied to study a serie of panels, presenting the comparison with the finite element results in terms of buckling loads, buckled configurations and interaction curves. The development of the formulation is discussed throughout the paper, including considerations on the symmetry and the anti-symmetry of the buckling shapes, making possible a significant reduction of the computational effort.

2 Formulation

The work deals with the study of the buckling behaviour of omega flat stiffened panels made of composite materials and subjected to combined in-plane loads. The formulation considers the case of a large structure undergoing local buckling so that the analysis can be performed referring to a smaller unit, representative of the behaviour of the overall structure [21–23]. In particular, the unit is composed of two stiffeners, one bay and two half-bays, as reported in Figure 1(a). The transverse edges of the panel are simply-supported, as the effect of the elasticity along these sides has a minor impact on the panel buckling load, while the longitudinal edges are subjected to periodic boundary conditions.

Only local buckling modes are investigated. The possible local buckling models present nodal lines along the intersections of the plate elements composing the panel. Global buckling modes, i.e. modes characterized by halfwaves encompassing several stiffeners, are not investigated.

The main idea of the present formulation is to represent the panel with a small number of plate elements, whose out of plane deflections are described with trigonometric shape functions. By introducing considerations regarding the symmetry and the anti-symmetry of the buckling modes, the model of Figure 1(a) is reduced to

the four plate element model of Figure 1(b). The IDs of the four elements are highlighted in the figure together with the longitudinal length a, which is common to all the elements composing the panel.

The generic plate element i is reported in Figure 2. A Cartesian coordinate system is taken over the midsurface of each plate element. The x-and y-axis are directed along the longitudinal and the transverse directions, while the midsurface corresponds to $z = 0$. The figure illustrates also the loading conditions of biaxial compression (or tension) and shear, that can be applied separately or in combination.

The panels here analyzed are thin, and the transverse shear strains are assumed negligible. They are composed of laminates with an arbitrary number of layers, under the assumptions of symmetric lay-up, i.e. $B_{ik} = 0$, and null membrane anisotropy, i.e. $A_{16} = A_{26} = 0$. On the other hand, the bending-twisting coupling terms D_{16} and D_{26} are not neglected, so that the formulation can be applied to the study of panels made of symmetric and balanced laminates. The constitutive equation of the generic plate is then [10]:

$$\begin{Bmatrix} N_{xx} \\ N_{yy} \\ N_{xy} \\ M_{xx} \\ M_{yy} \\ M_{xy} \end{Bmatrix} = \begin{bmatrix} A_{11} & A_{12} & 0 & 0 & 0 & 0 \\ A_{12} & A_{22} & 0 & 0 & 0 & 0 \\ 0 & 0 & A_{66} & 0 & 0 & 0 \\ 0 & 0 & 0 & D_{11} & D_{12} & D_{16} \\ 0 & 0 & 0 & D_{12} & D_{22} & D_{26} \\ 0 & 0 & 0 & D_{16} & D_{26} & D_{66} \end{bmatrix} \begin{Bmatrix} \epsilon_{xx} \\ \epsilon_{yy} \\ 2\epsilon_{xy} \\ -w_{,xx} \\ -w_{,yy} \\ -2w_{,xy} \end{Bmatrix} \tag{1}$$

where the terms A_{ik} and D_{ik} are the in-plane and bending stiffnesses, N_{ik} and M_{ik} are the internal forces and the moments per unit length, ϵ_{ik} are the components of the membrane strain tensor, and w is the out of plane displacement. The comma followed by the coordinate denotes the differentiation with respect to that coordinate.

2.1 Total potential energy

The problem is formulated referring to the principle of the minimum potential energy, and the method of Ritz is applied to obtain an approximate solution. The main advantage of adopting a variational formulation relies in the need of satisfying only the essential boundary conditions of the problem. Indeed, the natural conditions involving the equilibrium of the forces exchanged between the adjacent plates elements could be hardly fulfilled, as it would be required in the context of a strong form formulation.

The total potential energy of the panel is given by the sum of the contributions of the plate elements composing the section, so:

$$\Pi = \sum_{i}^{\mathrm{N_p}} \Pi_i + \sum_{i}^{\mathrm{N_c}} P_i \tag{2}$$

where $\mathrm{N_p}$ is the number of plates to discretize the section, $\mathrm{N_c}$ is the number of compatibility conditions, and P_i is a penalty term which is added to the functional to enforce the compatibility conditions between the adjacent

plates. The first term in the right-hand side of Eq. (3) is:

$$\Pi_i = U_b + V_{\text{load}} \tag{3}$$

where U_b is the strain energy for bending, and V_{load} is the potential energy of the external loads.
According to Kirchhoff thin plate theory, the bending energy reads:

$$\begin{aligned} U_b = \frac{1}{2}\int_\Omega \big(&D_{11}w_{,xx}^2 + 2D_{12}w_{,xx}w_{,yy} + D_{22}w_{,yy}^2 + 4D_{66}w_{,xy}^2 + \\ &+4D_{16}w_{,xx}w_{,xy} + 4D_{26}w_{,yy}w_{,xy}\big)\, d\Omega \end{aligned} \tag{4}$$

where Ω and w denote the surface and the out of plane displacement of the i-th plate element, respectively. The expression of Eq. (4) can be organized in a compact form as:

$$U_b = \frac{1}{2}\int_\Omega \mathbf{k}^T\mathbf{D}\mathbf{k}\, d\Omega \tag{5}$$

The term $\mathbf{k}$ of Eq. (5) is the vector of the curvatures of the plate element i, and is defined as:

$$\mathbf{k} = \{-w_{,xx} \quad -w_{,yy} \quad -2w_{,xy}\}^T \tag{6}$$

while the bending stiffness matrix $\mathbf{D}$, obtained from the classical lamination theory, is:

$$\mathbf{D} = \begin{bmatrix} D_{11} & D_{12} & D_{16} \\ D_{12} & D_{22} & D_{26} \\ D_{16} & D_{26} & D_{66} \end{bmatrix} \tag{7}$$

The potential of the external loads is expressed as the superposition of the different contributions due to the in-plane loads:

$$V_{\text{load}} = V_l + V_s + V_t \tag{8}$$

where V_l, V_s and V_t are the potential of the longitudinal, shear and transverse loads, respectively. Their expression is:

$$V_l = \frac{1}{2}\lambda N_x \int_\Omega w_{,x}^2\, d\Omega \qquad V_s = \lambda N_{xy}\int_\Omega w_{,x}w_{,y}\, d\Omega \qquad V_t = \frac{1}{2}\lambda N_y \int_\Omega w_{,y}^2\, d\Omega \tag{9}$$

where N_x and N_y are the pre-buckling longitudinal and transverse loads, considered positive in compression. The term N_{xy} is the pre-buckling shear load, taken positive according to the sign convention of Figure 2, while the scalar parameter λ is the multiplier of the pre-buckling configuration.

2.2 Pre-buckling stress distribution

The pre-buckling stress distribution is determined assuming that the forces per unit length are constant within each element composing the panel. The shear and the transverse loads are carried only by the elements 1 and

4 of Figure 1(b), therefore N_{xy} and N_y are directly defined as input data of the problem. The values of the axial load per unit length N_x are, in general, different from element to element. Introducing the assumption of common axial shortening, the axial load N_x on the stiffener and the foot is expressed as function of the value on the skin. In particular, the shortening of a plate element is determined by integrating the axial strain along the element length:

$$\Delta u = \int_0^a \epsilon_x \, dx \tag{10}$$

where Δu is the axial shortening, taken positive in compression. The relation between the axial strains ϵ_x and the membrane forces is obtained by inverting the membrane part of the laminate constitutive equation of Eq. (1):

$$\begin{Bmatrix} \epsilon_x \\ \epsilon_y \\ \gamma_{xy} \end{Bmatrix} = \begin{bmatrix} A^*_{11} & A^*_{12} & 0 \\ A^*_{12} & A^*_{22} & 0 \\ 0 & 0 & A^*_{66} \end{bmatrix} \begin{Bmatrix} N_x \\ N_y \\ N_{xy} \end{Bmatrix} \tag{11}$$

where the terms A^*_{ik} are the components of the laminate in-plane compliance matrix.

From Eqs. (10) and (11), the shortening of the generic element is obtained as:

$$\Delta u = a A^*_{11} N_x + a A^*_{12} N_y \tag{12}$$

Imposing the compatibility between the axial shortening of the skin and the other plate elements, and assuming that the stiffener is subjected only to axial loads, it is derived:

$$N_{x,\mathrm{st}} = \frac{A^*_{11,\mathrm{skin}} N_{x,\mathrm{skin}} + A^*_{12,\mathrm{skin}} N_{y,\mathrm{skin}}}{a_{11,\mathrm{st}}} \tag{13}$$

where the subscripts *st* and *skin* refer to the stiffener and the skin elements, respectively.

For a given pre-buckling loading condition, the transverse load $N_{y,\mathrm{skin}}$ can be expressed as function of $N_{x,\mathrm{skin}}$ by means of a nondimensional parameter ξ:

$$N_{y,\mathrm{skin}} = \xi N_{x,\mathrm{skin}} \tag{14}$$

It follows that Eq. (13) can be rewritten as:

$$N_{x,\mathrm{st}} = \Psi_{\mathrm{st}} N_{x,\mathrm{skin}} \tag{15}$$

where the term Ψ_{st} is:

$$\Psi_{\mathrm{st}} = \frac{A^*_{11,\mathrm{skin}} + \xi A^*_{12,\mathrm{skin}}}{A^*_{11,\mathrm{st}}} \tag{16}$$

The same steps can be performed to put in relation the pre-buckling axial force per unit length on the skin $N_{x,\mathrm{skin}}$ with the pre-buckling force in the foot region $N_{x,\mathrm{foot}}$. In this case, it results:

$$\Psi_{\mathrm{foot}} = \frac{A^*_{11,\mathrm{skin}} + \xi A^*_{12,\mathrm{skin}}}{A^*_{11,\mathrm{foot}}} \tag{17}$$

2.3 Foot modeling

The formulation accounts explicitly for the presence of the stiffener foot, i.e. the flange connecting the stiffener and the skin, allowing to reduce the level of approximation of the panel and, consequently, to improve the accuracy of the results.

The foot region has a width denoted as l_{foot}, and the lay-up is given by the superposition of the skin and the stiffener laminates. The approach here developed is based on the model of Figure 3, where the offset of the resulting laminate is assumed to be negligible. In general, the lay-up of this small area is unsymmetric, as it is obtained from the stacking of two lay-ups that are, in general, different. The unsymmetry of the lay-up is accounted for referring to the reduced bending stiffness method. The approach assumes as bending stiffness the matrix $\mathbf{D}^*$, defined as:

$$\mathbf{D}^* = \mathbf{D} - \mathbf{B}\mathbf{A}^{-1}\mathbf{B} \tag{18}$$

Thus, the bending energy related to the skin plate element, i.e. the element 1 of Figure 1(b), is obtained after splitting Eq. (5) into two contributions:

$$U_b = \frac{1}{2}\int_0^a \int_0^{l_{\text{foot}}} \mathbf{k}^T \mathbf{D}^* \mathbf{k}\, dxdy + \frac{1}{2}\int_0^a \int_{l_{\text{foot}}}^{b_1/2} \mathbf{k}^T \mathbf{D}\mathbf{k}\, dxdy \tag{19}$$

Similarly, the contribution of the axial load is obtained by dividing in the first of Eq. (9) the contribution due to the foot region and the skin:

$$V_l = \frac{1}{2} N_{x,\text{skin}} \left(\Psi_{\text{foot}} \int_0^a \int_0^{l_{\text{foot}}} w_{,x}^2\, dxdy + \int_0^a \int_{l_{\text{foot}}}^{b_1/2} w_{,x}^2\, dxdy \right) \tag{20}$$

2.4 Boundary conditions

The problem presents natural and essential boundary conditions. The natural conditions regard the equilibrium of the bending moments exchanged between the plate elements at the common edges. Thanks to the variational formulation, these conditions are enforced in a weak form, and are progressively satisfied as the number of shape functions is increased. On the other hand, the essential conditions should be imposed a priori. They regard the out of plane displacements along the four edges of the plate, the compatibility of the rotations along the longitudinal edges and the compatibility between the axial shortening of the different elements.

The first of the three conditions is related to the assumption of local buckling, meaning that the buckling modes are characterized by nodal lines in correspondence of the common edges of the different plate elements. This condition requires that the translation along the four edges of the plate element is null:

$$\begin{cases} w(x,y) = 0 \quad \text{for} \qquad x = 0, a \\ w(x,y) = 0 \quad \text{for} \qquad y = 0, b \end{cases} \tag{21}$$

The condition of Eq. (21) is identically satisfied through the choice of the shape functions described in the next section.

The second essential condition regards the compatibility of the rotations between adjacent elements. In the context of the Kirchhoff thin plate theory, the rotation coincides with the first derivative of the out of plane displacement. Denoting with i and j two generic adjacent plates, the condition on the rotations around the x-axis reads:

$$[w_{,y}(x,b)]_i - [w_{,y}(x,0)]_j = 0 \tag{22}$$

The condition of Eq. (22) involves the shape functions of different plate elements and is imposed using penalty terms. The compatibility between the axial shortening of the plate elements is ensured evaluating the pre-buckling stress distribution outlined in the previous section.

2.5 Ritz approximation

The solution strategy is based on the method of Ritz, describing the unknowns by shape functions that span the entire surface of the plate element.

The choice of the functions is based on the observation that the longitudinal edges are subjected to a restraint against the rotation, due to the interaction with the adjoining plate elements. As each element is subjected to a condition comprised between the two limiting cases of simply-supported and clamped edges, the shape functions are chosen as the superposition of two terms:

$$w = w^s + w^c \tag{23}$$

where w^s and w^c are the functions satisfying the simply-supported and the clamped conditions, respectively. The first term of Eq. (23) is:

$$w^s = \sum_{m,n}^{\alpha,\beta} q^s_{mn} \sin\frac{m\pi x}{a} \sin\frac{n\pi y}{b} = \sum_{m,n}^{\alpha,\beta} q^s_{mn}\phi_{mn} \tag{24}$$

where α and β are the number of terms along the longitudinal and the transverse directions, while the scalars q^s_{mn} are the corresponding amplitudes. The derivative of w^s with respect to the coordinate y is not null at the two longitudinal edges, meaning that the functions allow the rotation of the element.

The second term of Eq. (23) is taken as [24]:

$$w^c = \sum_{m,n}^{\alpha,\gamma} q^c_{mn} \sin\frac{m\pi x}{a} \left[\cos\frac{(n-1)\,\pi y}{b} - \cos\frac{(n+1)\,\pi y}{b}\right]\frac{1}{2} = \sum_{m,n}^{\alpha,\gamma} q^c_{mn}\varphi_{mn} \tag{25}$$

where α and γ are the number of shape functions along the two orthogonal directions x and y, and the terms q^c_{mn} define the amplitudes of the generic shape functions φ_{mn}. The functions of Eq. (25) are characterized by null derivative with respect to y along the two longitudinal edges, thus preventing the rotation of the element. It is straightforward to verify that the expressions of Eqs. (24) and (25) identically satisfy the essential boundary conditions of Eq. (21).

A matrix notation is now introduced to collect the unknown amplitudes of the i-th plate element into a single vector, defined as:

$$\mathbf{q} = \begin{Bmatrix} \mathbf{q}^s \\ \mathbf{q}^c \end{Bmatrix} \tag{26}$$

The two vectors $\mathbf{q}^s$ and $\mathbf{q}^c$ collect the unknown amplitudes of the functions of Eqs. (24) and (25), and are organized as:

$$\mathbf{q}^s = \begin{Bmatrix} q^s_{11} \\ q^s_{12} \\ \vdots \\ q^s_{\alpha\beta} \end{Bmatrix} \qquad \mathbf{q}^c = \begin{Bmatrix} q^c_{11} \\ q^c_{12} \\ \vdots \\ q^c_{\alpha\gamma} \end{Bmatrix} \tag{27}$$

The dimensions of the two vectors depend on the number of shape functions used to describe the out of plane displacement, and are equal to $\alpha \times \beta$ and $\alpha \times \gamma$, respectively.

According to the definition of Eq. (27), the trigonometric expansion of the out of plane displacement can be organized:

$$w = \begin{bmatrix} \boldsymbol{\phi} & \boldsymbol{\varphi} \end{bmatrix} \begin{Bmatrix} \mathbf{q}^s \\ \mathbf{q}^c \end{Bmatrix} = \begin{bmatrix} \boldsymbol{\phi} & \boldsymbol{\varphi} \end{bmatrix} \mathbf{q} \tag{28}$$

where the terms $\boldsymbol{\phi}$ and $\boldsymbol{\varphi}$ are row vectors, where the shape functions of Eqs. (24) and (25) are organized as:

$$\begin{aligned} \boldsymbol{\phi} &= [\phi_{11} \quad \phi_{12} \dots \phi_{\alpha\beta}] \\ \boldsymbol{\varphi} &= [\varphi_{11} \quad \varphi_{12} \dots \varphi_{\alpha\gamma}] \end{aligned} \tag{29}$$

For the skin element, the shape functions of Eq. (28) are substituted into the bending energy expression of Eq. (19), where the integration is split in the sum of two contributions in order to account for the different bending stiffnesses of the regions with and without the stiffener foot. For all the other elements, i.e the stiffener flange, the stiffener crown, and the portion of the skin under the stiffener, the expression of Eq. (28) is substituted into Eq. (5). The final expression can be written in the form:

$$U_b = \frac{1}{2} \begin{Bmatrix} \mathbf{q}^s \\ \mathbf{q}^c \end{Bmatrix}^T \begin{bmatrix} \tilde{\mathbf{K}}^s & \tilde{\mathbf{K}}^{sc} \\ \left(\tilde{\mathbf{K}}^{sc}\right)^T & \tilde{\mathbf{K}}^c \end{bmatrix} \begin{Bmatrix} \mathbf{q}^s \\ \mathbf{q}^c \end{Bmatrix} = \frac{1}{2} \mathbf{q}^T \tilde{\mathbf{K}} \mathbf{q} \tag{30}$$

where $\tilde{\mathbf{K}}$ is the bending stiffness matrix of the plate element, and the submatrices $\tilde{\mathbf{K}}^s$, $\tilde{\mathbf{K}}^c$ and $\tilde{\mathbf{K}}^{sc}$ are:

$$\tilde{\mathbf{K}}^s = \int_\Omega \begin{bmatrix} \boldsymbol{\phi}^T_{,xx} & \boldsymbol{\phi}^T_{,yy} & 2\boldsymbol{\phi}^T_{,xy} \end{bmatrix} \mathbf{D} \begin{bmatrix} \boldsymbol{\phi}_{,xx} \\ \boldsymbol{\phi}_{,yy} \\ 2\boldsymbol{\phi}_{,xy} \end{bmatrix} d\Omega \tag{31}$$

$$\tilde{\mathbf{K}}^c = \int_\Omega \begin{bmatrix} \boldsymbol{\varphi}^T_{,xx} & \boldsymbol{\varphi}^T_{,yy} & 2\boldsymbol{\varphi}^T_{,xy} \end{bmatrix} \mathbf{D} \begin{bmatrix} \boldsymbol{\varphi}_{,xx} \\ \boldsymbol{\varphi}_{,yy} \\ 2\boldsymbol{\varphi}_{,xy} \end{bmatrix} d\Omega \tag{32}$$

$$\tilde{\mathbf{K}}^{sc} = \int_\Omega \begin{bmatrix} \boldsymbol{\phi}_{,xx}^T & \boldsymbol{\phi}_{,yy}^T & 2\boldsymbol{\phi}_{,xy}^T \end{bmatrix} \mathbf{D} \begin{bmatrix} \boldsymbol{\varphi}_{,xx} \\ \boldsymbol{\varphi}_{,yy} \\ 2\boldsymbol{\varphi}_{,xy} \end{bmatrix} d\Omega \tag{33}$$

The potential of the longitudinal compression load is obtained by substituting Eq. (28) into Eqs. (20) and (9) for the skin and the stiffener elements, respectively. The resulting expression is:

$$V_l = \frac{1}{2}\lambda \Psi N_{x,\text{skin}} \begin{Bmatrix} \mathbf{q}^s \\ \mathbf{q}^c \end{Bmatrix}^T \begin{bmatrix} \int_\Omega \boldsymbol{\phi}_{,x}^T \boldsymbol{\phi}_{,x} d\Omega & \int_\Omega \boldsymbol{\phi}_{,x}^T \boldsymbol{\varphi}_{,x}\, d\Omega \\ \int_\Omega \boldsymbol{\varphi}_{,x}^T \boldsymbol{\phi}_{,x} d\Omega & \int_\Omega \boldsymbol{\varphi}_{,x}^T \boldsymbol{\varphi}_{,x}\, d\Omega \end{bmatrix} \begin{Bmatrix} \mathbf{q}^s \\ \mathbf{q}^c \end{Bmatrix} = \frac{1}{2}\lambda \mathbf{q}^T \mathbf{G}^{\text{axial}} \mathbf{q} \tag{34}$$

where $\Psi = \Psi_{\text{st}}$ for the stiffener elements, and $\Psi = 1$ otherwise.

Similarly, the expression of the shear load is obtained by substituting Eq. (28) into the second expression of Eq. (9), leading to:

$$V_s = \frac{1}{2}\lambda N_{xy} \begin{Bmatrix} \mathbf{q}^s \\ \mathbf{q}^c \end{Bmatrix}^T \begin{bmatrix} \int_\Omega \boldsymbol{\phi}_{,x}^T \boldsymbol{\phi}_{,y} d\Omega & \frac{1}{2}\int_\Omega \left(\boldsymbol{\phi}_{,x}^T \boldsymbol{\varphi}_{,y} + \boldsymbol{\phi}_{,y}^T \boldsymbol{\varphi}_{,x} \right) d\Omega \\ \frac{1}{2}\int_\Omega \left(\boldsymbol{\varphi}_{,x}^T \boldsymbol{\phi}_{,y} + \boldsymbol{\varphi}_{,y}^T \boldsymbol{\phi}_{,x} \right) d\Omega & \int_\Omega \boldsymbol{\varphi}_{,x}^T \boldsymbol{\varphi}_{,y}\, d\Omega \end{bmatrix} \begin{Bmatrix} \mathbf{q}^s \\ \mathbf{q}^c \end{Bmatrix} = \frac{1}{2}\lambda \mathbf{q}^T \mathbf{G}^{\text{shear}} \mathbf{q} \tag{35}$$

As the shear load is not carried by the stiffener, the contribution of Eq. (35) is computed for the skin elements only.

The contribution of the applied loads is related to the transverse compression. Referring to Eq. (28) and to the last expression of Eq. (9), it is:

$$V_t = \frac{1}{2}\lambda N_y \mathbf{q}^T \begin{bmatrix} \int_\Omega \boldsymbol{\phi}_{,y}^T \boldsymbol{\phi}_{,y} d\Omega & \int_\Omega \boldsymbol{\phi}_{,y}^T \boldsymbol{\varphi}_{,y}\, d\Omega \\ \int_\Omega \boldsymbol{\varphi}_{,y}^T \boldsymbol{\phi}_{,y} d\Omega & \int_\Omega \boldsymbol{\varphi}_{,y}^T \boldsymbol{\varphi}_{,y}\, d\Omega \end{bmatrix} \mathbf{q} = \frac{1}{2}\lambda \mathbf{q}^T \mathbf{G}^{\text{trans}} \mathbf{q} \tag{36}$$

Even in this case, the contribution of Eq. (36) is computed only for the skin elements.

It is worth noting that the matrices of Eqs. (31)-(36) require the calculation of integrals involving the products between the derivatives of the trigonometric functions $\boldsymbol{\phi}$ and $\boldsymbol{\varphi}$. This operation, due to the regularity of the domain, are performed analytically and numerical integration is not needed, and all of the terms of the matrices can be obtained in a closed-form manner.

Having established the expression of the bending energy and the potential of the external loads, it is possible to derive the equilibrium equations by applying the minimum potential energy principle. Referring to Eqs. (3), (8) and (26), the minimization of the total potential energy requires that:

$$\frac{\partial \Pi_i}{\partial \mathbf{q}} = \frac{\partial U_b}{\partial \mathbf{q}} + \frac{\partial (V_l + V_s + V_t)}{\partial \mathbf{q}} = 0 \tag{37}$$

The right hand side of Eq. (37) highlights two terms, the plate bending matrix and the loading stiffness matrix. The former is derived from the contribution of the bending energy, the latter from the external loads.

The first term of Eq. (37) is obtained referring to Eq. (4):

$$\frac{\partial U_b}{\partial \mathbf{q}} = \tilde{\mathbf{K}}\mathbf{q} \tag{38}$$

The second term of Eq. (37) is derived from Eqs. (34), (35) and (36). The derivatives with respect to the unknown amplitudes are:

$$\frac{\partial V_l}{\partial \mathbf{q}} = \lambda \mathbf{G}^{\text{axial}}\mathbf{q} \qquad \frac{\partial V_s}{\partial \mathbf{q}} = \lambda \mathbf{G}^{\text{shear}}\mathbf{q} \qquad \frac{\partial V_t}{\partial \mathbf{q}} = \lambda \mathbf{G}^{\text{trans}}\mathbf{q} \tag{39}$$

The total contribution of the external load can be re-arranged as:

$$\frac{\partial V_{\text{load}}}{\partial \mathbf{q}} = \frac{\partial \left(V_l + V_s + V_t\right)}{\partial \mathbf{q}} = \lambda \mathbf{G}\mathbf{q} \tag{40}$$

where $\mathbf{G}$ is the load stiffness matrix of the plate element i, given by the sum of the contribution of the three loads here considered:

$$\mathbf{G} = \mathbf{G}^{\text{axial}} + \mathbf{G}^{\text{shear}} + \mathbf{G}^{\text{trans}} \tag{41}$$

2.6 Symmetric and anti-symmetric buckling patterns

The number of shape functions necessary to represent the deflected surface of each plate element can be significantly reduced by introducing considerations related to the symmetries of the buckling modes. A plate element loaded in uniform biaxial compression and shear, and subjected to equal constraints at the two parallel edges, can display two distinct buckling patterns:

- symmetric, i.e. the sum of the longitudinal and the transverse halfwaves is even
- anti-symmetric, i.e. the sum of the longitudinal and the transverse halfwaves is odd

Similar considerations were introduced by Stein and Neff [25] for the study of the shear buckling of isotropic panels, and by Rastogi [26] for the study of composite panels under biaxial compression and shear.

The existence of two possible buckled configurations allows to divide the vector of the unknowns amplitudes into two independent sets, called $\overline{\mathbf{q}}_{i,S}$ and $\overline{\mathbf{q}}_{i,A}$, where the subscript S stands for symmetric and A for anti-symmetric.

The first vector $\overline{\mathbf{q}}_{i,S}$ collects the symmetric amplitudes, while the second $\overline{\mathbf{q}}_{i,A}$ the anti-symmetric ones. The two vectors can be put in relation to the global vector $\overline{\mathbf{q}}_i$ that includes both the symmetric and the anti-symmetric components introducing the transformation matrices $\mathbf{T}_{i,S}$ and $\mathbf{T}_{i,A}$:

$$\mathbf{q}_i = \mathbf{T}_{i,S}\overline{\mathbf{q}}_{i,S} \qquad \mathbf{q}_i = \mathbf{T}_{i,A}\overline{\mathbf{q}}_{i,A} \tag{42}$$

From the partitioning of the amplitudes of the simply-supported and clamped functions of Eq. (26), it follows that the matrices $\mathbf{T}_{i,S}$ and $\mathbf{T}_{i,A}$ take the form:

$$\mathbf{T}_{i,S} = \begin{bmatrix} \mathbf{T}^s_{i,S} & \mathbf{0} \\ \mathbf{0} & \mathbf{T}^c_{i,S} \end{bmatrix} \qquad \mathbf{T}_{i,A} = \begin{bmatrix} \mathbf{T}^s_{i,A} & \mathbf{0} \\ \mathbf{0} & \mathbf{T}^c_{i,A} \end{bmatrix} \tag{43}$$

The matrices $\mathbf{T}_{i,S}$ and $\mathbf{T}_{i,A}$ allow for a formally convenient representation of the element stiffness matrices in terms of symmetric and anti-symmetric terms only, and are used in the next section to derive the equations governing the local buckling of the omega stiffened panel.

Referring to the panel of Figure 1, it can be observed that symmetry considerations apply to the buckled pattern of the elements representing the skin of the panel and the crown of the stiffener. Indeed, these two elements are supported at the opposite edges by identical plate elements that consequently provide the same level of rotational restraint. On the other hand, the elements representing the lateral webs of the stiffeners are supported along the transverse edges by different elements, each of them furnishing a different level of restraint at the two opposite longitudinal edges. Therefore, no assumptions can be introduced a priori on the buckling deflection of the web elements that, consequently, are characterized by the superposition of both symmetric and anti-symmetric terms.

2.7 Assembly of the global equation system

The representative unit of Figure 1(a) consists of eleven plate elements. However, the periodicity of the buckling deflections allows to reduce the total number of the plate elements. The reduction is done by considering the simpler model of Figure 1(b), which is composed of four plate elements only. The model assumes that the buckling modes of the elements 1, 3 and 4 are symmetric or anti-symmetric, while no symmetry is expected for the element 2, whose deflections are characterized by a pattern with symmetric and anti-symmetric components. The combinations of feasible buckling modes respecting the symmetries of the problem are summarized in Table 1.

It is worth noting that the total potential energy stored in the eleven-plate elements model of Figure 1(a) is exactly four times the potential energy of the reduced model of Figure 1(b). Therefore, the minimization of the potential energy of the structure of Figure 1(a) implies the minimization of the energy of the structure of Figure 1(b).

The vector of the unknowns of the four-plate model is introduced as:

$$\mathbf{q} = \begin{Bmatrix} \mathbf{q}_1 \\ \mathbf{q}_2 \\ \mathbf{q}_3 \\ \mathbf{q}_4 \end{Bmatrix} \tag{44}$$

where the subscript denotes the plate element number, according to the numbering of Figure 1(b). Each of the vectors $\mathbf{q}_i$ includes the symmetric and the anti-symmetric terms according to the definition of Eq. (26), and has dimension that depends on the number of shape functions used to represent the out of plane displacement.

The bending stiffness matrix of the panel is obtained by assembling the matrices $\tilde{\mathbf{K}}$ relative to the four plate

elements of Figure 1(b) is:

$$\tilde{\mathbf{K}} = \frac{1}{2}\begin{bmatrix} \tilde{\mathbf{K}}_1 & \mathbf{0} & \mathbf{0} & \mathbf{0} \\ \mathbf{0} & 2\tilde{\mathbf{K}}_2 & \mathbf{0} & \mathbf{0} \\ \mathbf{0} & \mathbf{0} & \tilde{\mathbf{K}}_3 & \mathbf{0} \\ \mathbf{0} & \mathbf{0} & \mathbf{0} & \tilde{\mathbf{K}}_4 \end{bmatrix} \tag{45}$$

The terms related to the elements 1, 3 and 4 are divided by a factor of 2 in agreement with their half-width. The same assembly procedure is performed for the three components of the loading stiffness matrices:

$$\mathbf{G}^{\text{axial}} = \frac{1}{2}\begin{bmatrix} \mathbf{G}_1^{\text{axial}} & \mathbf{0} & \mathbf{0} & \mathbf{0} \\ \mathbf{0} & 2\mathbf{G}_2^{\text{axial}} & \mathbf{0} & \mathbf{0} \\ \mathbf{0} & \mathbf{0} & \mathbf{G}_3^{\text{axial}} & \mathbf{0} \\ \mathbf{0} & \mathbf{0} & \mathbf{0} & \mathbf{G}_4^{\text{axial}} \end{bmatrix} \tag{46}$$

$$\mathbf{G}^{\text{shear}} = \frac{1}{2}\begin{bmatrix} \mathbf{G}_1^{\text{shear}} & \mathbf{0} & \mathbf{0} & \mathbf{0} \\ \mathbf{0} & \mathbf{0} & \mathbf{0} & \mathbf{0} \\ \mathbf{0} & \mathbf{0} & \mathbf{0} & \mathbf{0} \\ \mathbf{0} & \mathbf{0} & \mathbf{0} & \mathbf{G}_4^{\text{shear}} \end{bmatrix} \tag{47}$$

$$\mathbf{G}^{\text{trans}} = \frac{1}{2}\begin{bmatrix} \mathbf{G}_1^{\text{trans}} & \mathbf{0} & \mathbf{0} & \mathbf{0} \\ \mathbf{0} & \mathbf{0} & \mathbf{0} & \mathbf{0} \\ \mathbf{0} & \mathbf{0} & \mathbf{0} & \mathbf{0} \\ \mathbf{0} & \mathbf{0} & \mathbf{0} & \mathbf{G}_4^{\text{trans}} \end{bmatrix} \tag{48}$$

where the contributions of the shear and the transverse loads, which are carried only by the skin elements, are null in correspondence of the elements 2 and 3.

The panel load stiffness is finally derived by summing the three terms of Eq. (46), (47) and (48):

$$\mathbf{G} = \mathbf{G}^{\text{axial}} + \mathbf{G}^{\text{shear}} + \mathbf{G}^{\text{trans}} \tag{49}$$

The matrices $\tilde{\mathbf{K}}$ and $\mathbf{G}$ do not account for the boundary conditions of Eq. (22), which are imposed adopting a penalty approach. A torsion spring is introduced along the common edges of the plates, and the corresponding strain energy is related to the difference of rotation between the two elements. The compatibility requirement is automatically enforced by the total potential energy minimization process.

Denoting two generic adjacent plate elements with the letters i and j, the penalty strain energy $U_{p,ij}$ due to the difference of rotation at the common edge of the two plates is:

$$U_{p,ij} = \frac{k_t}{2}\int_0^a \left\{ \left[w_{,y}(x,b)\right]_i - \left[w_{,y}(x,0)\right]_j \right\}^2 dx \tag{50}$$

where k_t is the penalty stiffness of the spring.

From the expression of the shape functions of Eqs. (24) and (25), it is noted that only the simply-supported

terms provide a not null contribution to Eq. (50). The clamped terms are characterized, by definition, by null rotation at the edges.

Referring to Figure 1(b), the compatibility conditions to be imposed on the rotations regard the panel edges 3 and 2, 1 and 4, 1 and 2. Thus, the total penalty term is:

$$U_p = U_{p,23} + U_{p,41} + U_{p,21} \tag{51}$$

and the first derivative is:

$$\frac{\partial U_p}{\partial \mathbf{q}} = \mathbf{P}\mathbf{q} \tag{52}$$

The total stiffness matrix of the problem is finally obtained as the sum of the terms related to the bending stiffness of the panel of Eq. (45), and the terms related to the compatibility requirements on the rotations of Eq. (52):

$$\mathbf{K} = \tilde{\mathbf{K}} + \mathbf{P} \tag{53}$$

Referring to Eq. (49), the eigenvalue problem can be written as:

$$\left(\mathbf{K} + \lambda \mathbf{G}\right) \mathbf{q} = \mathbf{0} \tag{54}$$

From a mathematical point of view, the extra-diagonal terms of Eq. (52) determine the coupling between the degrees of freedom of the four plate elements. The deflection of an element tends to induce the deflection of the adjacent elements through the compatibility requirements.

The problem of Eq. (54) does not account for the considerations regarding the symmetry and anti-symmetry of the buckling modes of the elements 1, 3 and 4. The problem is split to study, separately, the eight admissible configurations of Table 1.

The matrices $\mathbf{T}_i$ of Eq. (42), built for the single plate element, are assembled into a unique matrix related to the global vector of unknowns of Eq. (44). The transformation matrix related to the first configuration of Table 1 is then:

$$\mathbf{T}_{SSS} = \begin{bmatrix} \mathbf{T}_{1,S} & \mathbf{0} & \mathbf{0} & \mathbf{0} \\ \mathbf{0} & \mathbf{I} & \mathbf{0} & \mathbf{0} \\ \mathbf{0} & \mathbf{0} & \mathbf{T}_{3,S} & \mathbf{0} \\ \mathbf{0} & \mathbf{0} & \mathbf{0} & \mathbf{T}_{4,S} \end{bmatrix} \tag{55}$$

The identity matrix is inserted in correspondence of the degrees of freedom of the plate element 2, for which no symmetries are expected, and all the degrees of freedom are maintained. The transformation matrices corresponding to the other seven configurations of Table 1 are $\mathbf{T}_{SSA}$, $\mathbf{T}_{SAS}$, $\mathbf{T}_{SAA}$, $\mathbf{T}_{ASS}$, $\mathbf{T}_{ASA}$, $\mathbf{T}_{AAS}$, $\mathbf{T}_{AAA}$ and are built in a similar way of Eq. (55).

Denoting with $\mathbf{T}$ the generic transformation matrix, the relation between the complete vector of unknowns of Eq. (44) and the reduced one is:

$$\mathbf{q} = \mathbf{T}\overline{\mathbf{q}} \tag{56}$$

where $\overline{\mathbf{q}}$ is the vector of unknowns reduced to the symmetric and the anti-symmetric terms only.
From Eq. (56), the stiffness and the loading stiffness matrices of Eqs. (49) and (53) transform as:

$$\overline{\mathbf{K}} = \mathbf{T}^T\mathbf{K}\mathbf{T} \qquad \overline{\mathbf{G}} = \mathbf{T}^T\mathbf{G}\mathbf{T} \tag{57}$$

The buckling analysis of the structure is so reduced to the solution of eight eigenvalue problems in the form:

$$\left(\overline{\mathbf{K}} + \lambda\overline{\mathbf{G}}\right)\overline{\mathbf{q}} = \mathbf{0} \tag{58}$$

The smallest eigenvalue among the first ones obtained from the solution of the eight buckling problems identifies the buckling condition and the corresponding eigenvector defines the buckling mode.

3 Results

The analytical formulation is applied to study panels with different lay-ups, and subjected to conditions of biaxial and shear loadings, applied separately or in combination. The accuracy of the analytical results is discussed by comparing the results with those obtained from finite element analyses, both in terms of buckling forces and corresponding eigenmodes.
The effects of the foot on the panel buckling behaviour are assessed by presenting the results obtained with and without stiffener foot modeling. The convergence of the solution is then discussed with reference to the adopted shape functions.

3.1 Description of the panels

The panels under investigation are made from carbon epoxy unidirectional IM7/8552, whose ply properties are reported in Table 2.
Four different configurations are considered in terms of skin and stiffener lay-ups, as summarized in Table 3. The total number of plies is the same for all the panels, with 8 plies for the skin and 7 for the stiffener. The corresponding thicknesses are 1.0 mm and 0.875 mm, respectively.
The first three panels of Table 3 differ only for the skin lay-up. In particular, the panels denoted as QI1 and QI2 are characterized by a quasi-isotropic skin, while AP has an angle-ply skin. The panel CP is a cross-ply configuration, where the skin and the stiffener lay-ups have only plies at 0° and 90°. The first three panels present bending-twisting coupling. According to the nondimensional parameters proposed by Nemeth [27], the panels QI1 and CP are those characterized by the highest degree of flexural anisotropy, while only a slight level of anisotropy is observed for the panel QI2, as the ±45° plies are close to the plane of symmetry of the laminate.
The panels have longitudinal length of 550 mm and, referring to Figure 3, the dimensions b_2, b_3, and b_4 of the omega stiffener are 33.10 mm, 27.50 mm and 55.50 mm. The foot width is taken equal to 0.1 b_1. Different

values are considered for the skin width b_1 in order to study panels with different aspect ratios r, here defined as the ratio between the panel length and the distance from stiffener to stiffener:

$$r = \frac{a}{b_1} \tag{59}$$

3.2 Comparison with finite element analyses

The semi-analytical results are compared with Abaqus eigenvalue analyses [28]. The finite element models are realized using four-noded S4R shell elements whose size is chosen according to preliminary convergence analyses. The meshes are realized by modeling the unit of Figure 1(a), which is composed of two stiffeners, one bay and the two external half-bays. A multi-point constraint equation is introduced to impose the continuity of the transverse displacements and the rotations at the nodes of the two longitudinal edges.

Compression loads

The first set of results deals with loading conditions of pure compression. The buckling behaviour of the four panels of Table 3 is presented in Figure 4, where the aspect ratio r is plotted versus the nondimensional buckling load $k_{x,\text{buck}}$, defined as:

$$k_{x,\text{buck}} = \frac{N_{x,\text{buck}} b_1^2}{\pi^2 \sqrt{D_{11} D_{22}}} \tag{60}$$

where $N_{x,\text{buck}}$ is the buckling force per unit length on the skin of the panel. Similarly, the bending stiffnesses D_{11} and D_{22} are referred to the skin lay-up.

The analytical results of Figure 4 illustrate the agreement with the Abaqus analyses, with differences on the buckling loads below 5%. In the curve of Figure 4(c), a sudden drop of the nondimensional buckling load $k_{x,\text{buck}}$ is observed for aspect ratios greater than 5, and the buckling force per unit length progressively reduces as the aspect ratio is increased. This behaviour is explained observing the buckling modes of the panels with aspect ratios equal to 5 and 6 reported Figure 5. The figure presents the comparison with the results obtained in Abaqus, demonstrating the quality of the semi-analytical results also in terms of buckling modes. Figures 5(a) and 5(b) display an eigenmode governed by the deflection of the skin, corresponding to the region of the curve of Figure 4(c) before the drop of the nondimensional buckling load $k_{x,\text{buck}}$. Figures 5(c) and 5(d) highlight a different behaviour, where the buckling deflections regard almost exclusively the stiffener elements. This is the buckling mode obtained for aspect ratios greater than 5. The difference between the two modes explains the drop observed in Figure 4(c), which corresponds to a sudden transition from a skin to a stiffener instability.

Shear loads

The results for the shear buckling behaviour are shown in Figure 6, where the four panels are loaded with a positive shear. The buckling load is plotted in terms of the nondimensional parameter $k_{xy,\text{buck}}$, defined as:

$$k_{xy,\text{buck}} = \frac{N_{xy,\text{buck}} b_1^2}{\pi^2 \sqrt{D_{11} D_{22}}} \tag{61}$$

The results reveal percent differences between the semi-analytical and numerical predictions below 2%. Compared to the case of compression loads, local stiffener buckling is not observed, due to the fact that all the shear is carried by the skin.

Further results regarding the buckling under pure shear loads are summarized in Table 4 for panels with aspect ratio equal to 3. In this case, the shear is applied both in positive and negative direction. It can be observed that the sign of the load has high impact on the buckling forces of the first and the third configurations, which are the ones characterized by the highest degree of flexural anisotropy. No distinction exists between positive and negative shear loads for the cross-ply configuration. Even in this case, the semi-analytical buckling forces are in good agreement with the numerical ones, with a maximum difference of approximately 6%.

Combined loads

Table 5 summarizes the results obtained for the panels with aspect ratio equal to 3, loaded in compression and shear. Four different ratios between the pre-buckling axial and shear loads are considered, with N_x/N_{xy} equal to 0.25, 0.50, 1.0 and 2.0. The first two loading conditions are characterized by a prevalent contribution due to the shear. The third condition presents an equal contribution of shear and compression, while the fourth one is a compression-dominated load condition. Even in this case, the agreement between semi-analytical and finite element results is satisfactory, with percent differences below 6%.

The semi-analytical and the finite element buckling modes of the panel QI1 are reported in Figures 7 and 8, respectively. The results refer to the four loading conditions of panel QI1 presented in Table 5. The most relevant difference can be observed in the pattern associated to the loading condition with $N_x/N_{xy} = 0.25$, reported in Figures 7(a) and 8(a). The number of halfwaves is correctly predicted by the semi-analytical model, but the angle of skew is slightly overestimated compared to the Abaqus results. The other three ratios of compression and shear loads lead to almost identical buckling modes, both in terms of number of halfwaves as well as pattern skew. The number of halfwaves changes from four to five as the pre-buckling ratio N_x/N_{xy} is increased from 0.5 to 1.0. This effect is correctly captured by the semi-analytical model, as revealed by the comparison between Figures 7(c) and 8(c).

Biaxial loading conditions are presented in Table 6, where the buckling loads are reported for panels with aspect ratio of 3. The results consider two different loading conditions characterized by ratios between the longitudinal and transverse compression of 0.5 and 2.0. For the examined configurations, the percent differences between the

numerical and the analytical results are lower than 9%, slightly higher compared to the case of compression and shear only. This behaviour is explained observing that the introduction of the load in the y-direction determines a pre-buckling deformed shape characterized by a global bending of the panel in the xz-plane, with a consequent small deviation from the pre-buckling uniformity of N_x assumed in the semi-analytical model.

The interaction curves for biaxial compression loads are shown in Figure 9 for the four panels with aspect ratio $r = 4$. The semi-analytical results are plotted together with the Abaqus results, and a maximum percent difference of 8% is achieved for a given ratio of pre-buckling load. It is interesting to observe the different shape of the curve obtained depending on the lay-up of the skin. The curves of Figures 9(a)-9(c) are characterized by an almost flat initial region. This means that the longitudinal compression determines a slight reduction of the transverse buckling load until a certain ratio N_x/N_y. For instance, the curve of Figure 9(a) reveals that the reduction of N_y is very small for values of N_x/N_y below 1. The length of the initially flat portion of the curve is proportional to the amount of anisotropy of the skin lay-up. Indeed, the two panels QI1 and AP, that are the ones characterized by the highest degree of flexural anisotropy, display this behaviour more clearly. On the other hand, the cross-ply configuration CP, whose response is reported in Figure 9(d), presents a different response, and a noticeable reduction of the buckling load N_y is obtained even for small amounts of longitudinal load N_x.

Multi-axial loading conditions are considered in Figure 10, where loading condition of shear and biaxial tension/compression are considered for the four panel lay-ups, and assuming an aspect ratio of $r = 4$. Each curve reports the longitudinal load in abscissa and the shear load in ordinate. The curves are parametrized on the value of ξ, which is defined as the ratio between the transverse load N_y and the axial load N_x, as reported in Eq. (14). The value $\xi = 0$ denotes pure shear and compression conditions, while $\xi = 0.5$ denotes a multiaxial condition with shear, longitudinal compression and transverse compression equal to $N_y = 0.5N_x$. The curves relative to $\xi = -0.5$ consider shear, longitudinal compression and transverse traction equal to $N_y = -0.5N_x$.

Abaqus results are also reported in Figure 10 for a discrete number of points, revealing the ability of the semi-analytical method to predict, with a satisfactory level of accuracy, the shape of the interaction curve. As expected, the presence of a transverse tension tends to enlarge the stability region in comparison with the pure shear compression curve. The plots reveal the stiffening effect due to the anisotropy of the skin lay-ups. It can be observed that the compressive load increases or decreases depending on the sign of the shear. The three curves of Figures 10(a)-10(c) are not symmetric with respect to the x-axis, revealing the stiffening effect due to shear when applied in the weaker-in-bending stiffness diagonal of the skin laminate. On the opposite, the interaction curves of the cross-ply configuration of Figure 10(d) are symmetric with respect to the x-axis due to panel flexural isotropy.

The computational time for a typical Abaqus eigenvalue analysis, on a Intel Core Duo with 3.0 GHz and 8 GB of RAM, is of the order of 100 s. The semi-analytical solution is computed in less than 1 s, corresponding to a

speed-up around 100.

3.3 Effects due to the stringer foot

The effects of the stiffener foot on the panel buckling response are now assessed. The study is conducted by analyzing panels with different foot widths and subjected to compression loads. The stiffener dimensions are kept constant, and are those reported in Section 3.1, while the panel dimension b_1 is varied to consider different aspect ratios.

The results are reported in Figure 11, and are computed for each of the four lay-ups of Table 3. The curves report the nondimensional buckling load k_x, as defined in Eq. (60), versus the aspect ratio r, presenting the comparison between three stiffener foot configurations. The first one, whose results are identified by the thin continuous line, corresponds to a panel where the foot is neglected. The second configuration, described by a thick continuous line, has a foot width equal to 10% of the dimension b_1, the same ratio which has been hitherto considered. The third configuration, reported with the dash-dot curve, is relative to a panel with an increased width of $0.2\,b_1$.

The results reveal a noticeable difference between the nondimensional buckling loads obtained with or without the stiffener foot. Depending on the lay-up of the panel, the buckling load obtained by neglecting the foot can be highly conservative. Clearly, the differences increase with the dimensions of the foot. This behaviour is particularly evident in Figure 11(a), but the conservativeness of the predictions obtained without foot modeling are observed also in Figures 11(b)-11(d).

In terms of structural behaviour, there are two aspects to explain how the stiffener foot tends to increase the buckling force of the skin. Firstly, it increases the amount of restraint of the skin rotation along the longitudinal edges. Secondly, it tends to reduce the equivalent width of the skin involved in the buckling deflection, a concept sometimes introduced to approximately account for the presence of the foot. With this regard, it is useful to refer to a simplified model, where only the skin is considered. The compressive buckling force per unit length can be written as [16, 29]:

$$N_{x,\mathrm{buck}} = \left(\frac{\pi}{b}\right)^2 \left[\delta_1 \sqrt{D_{11} D_{22}} + \delta_2 \left(D_{12} + 2D_{66}\right)\right] \tag{62}$$

where δ_1 and δ_2 are scalar parameters, whose values depend on the boundary conditions along the longitudinal edges. The term b is the equivalent width of the skin, i.e. the portion of the skin assumed to contribute to the buckling out of plane displacements.

The formula of Eq. (62), due to the inverse proportionality relation between $N_{x,\mathrm{buck}}$ and the square of the panel width b, explains why the introduction of the foot determines an increase of the skin buckling force per unit length.

A common approach to account for the presence of the foot consists in applying Eq. (62) and choosing a value

of b in the range $(b_1 - 2l_{\text{foot}}) \leq b \leq b_1$. According to the concept of equivalent width, the ratio between the nondimensional buckling parameter $k_{x,\text{buck}}$, computed with and without the stiffener foot, can be determined by substituting Eq. (62) into Eq. (60) and is:

$$\frac{k_{x,\text{buck}}^{\text{foot}}}{k_{x,\text{buck}}^{\text{nofoot}}} = \frac{b_1^2}{b^2} \tag{63}$$

The comparison between the results of Figure 11 and Eq. (63) illustrates the inadequacy of an approach based on the equivalent width concept. Indeed, the curves of Figure 11 reveal the dependence of the ratio $k_{x,\text{buck}}^{\text{foot}}/k_{x,\text{buck}}^{\text{nofoot}}$ on the panel lay-up, while this effect cannot be captured by the formula of Eq. (63). This result puts in evidence the importance of adopting a plate assembly model where the stringer foot is accounted for.

3.4 Convergence of the solution

The number of shape functions used to describe the out of plane displacement is important to guarantee the convergence of the solution and an appropriate description of the buckled surface. In the literature, some formulations consider a trigonometric expansion of the out of plane displacement accounting for simply-supported terms only [23, 30]. The advantage of restricting the shape functions to simply-supported terms relies in the simplicity of the integrals to be performed to build the stiffness matrices. However, in absence of flexural twisting coupling, the use of sine terms only does not allow the exchange of bending moments between adjacent plates, and the natural boundary conditions cannot be satisfied even in a weak form. The superposition of clamped and simply-supported terms allows to overcome this limitation, making possible the fulfillment of the natural boundary conditions as the number of shape functions is increased. It is interesting to compare the results obtained representing the out of plane displacement as the sum of sine terms only, and those obtained assuming the superposition of simply-supported and clamped terms. The convergence of the buckling load is reported in Figure 12 for the panel QI1 subjected to a loading condition of combined compression and shear. The comparison is presented by reporting the results calculated with the present formulation with and without the clamped terms of Eq. (23). The number of clamped terms γ is taken equal to 2, while β is progressively increased from 2 to 15. The buckling load per unit length N_x^{buck}, normalized with respect to the finite element one $N_x^{\text{FE,buck}}$, is plotted versus the number of total degrees of freedom in Figure 12.

The figure illustrates that a number of 225 degrees of freedom ensures the convergence of the solution when clamped and simply-supported shape functions are used. On the other hand, the convergence significantly slows down when clamped functions are neglected, and the solution converges to its asymptotic value after about 375 degrees of freedom. The convergence value is 4% higher compared to that one obtained accounting for the clamped terms, as a consequence of the inability of the simply-supported shape functions to progressively satisfy the natural boundary conditions.

4 Conclusions

A semi-analytical method for the evaluation of the buckling response of omega stiffened panels subjected to multi-axial loads has been presented. The method considers a plate assembly representation of the structure, where the attachment between the skin and the stiffener is explicitly modeled. The formulation relies on the minimum potential energy principle, applied in conjunction with the method of Ritz. The numerical effectiveness of the formulation is maximized by exploiting the symmetries and the anti-symmetries of the buckling modes, and by the use of shape functions obtained from the superposition of simply-supported and clamped terms. This ensures a quick convergence of the solution with a computational speed-up, compared to finite elements, around 100. The comparison with the numerical results, presented for a wide range of panel lay-ups and aspect ratios, reveals differences below 9% for the buckling load and good agreement in terms of buckling pattern.

The importance of introducing the stiffener foot is assessed by illustrating the conservativeness of the buckling loads obtained with no foot, as well as the inadequacy of the simplified model based on the equivalent width concept.

The present formulation offers also the advantage of capturing local instabilities and relies on the possibility of accounting for multi-axial loads, which typically characterize the stress state of the aeronautical panels. It allows to quickly trace interaction curves for different combinations of loads, perform sensitivity studies, design optimization and, in general, to understand the effect of various design parameters, including the stiffener geometry or the lamination lay-ups.

References

[1] Stroud WJ, Greene WH, Anderson MS. Buckling loads of stiffened panels subjected to combined longitudinal compression and shear: results obtained with PASCO, EAL and STAGS computer programs. TP 2215, NASA, 1984.

[2] Lynch C, Murphy A, Price M, Gibson A. The computational post buckling analysis of fuselage stiffened panels loaded in compression. Thin-Walled Structures 2004;41(10):1445–1464.

[3] Cheung YK. Finite strip method in structural analysis. Oxford: Pergamon Press, 1976.

[4] Cheung YK, Kong J. Vibration and buckling of thin-walled structures by a new finite strip. Thin-Walled Structures 1995;21(4):327–343.

[5] Loughlan J. The buckling performance of composite stiffened panel structures subjected to combined in-plane compression and shear loading. Composite Structures 1994;29(2):197–212.

[6] Wang W, Guo S, Chang N, Yang W. Optimum buckling design of composite stiffened panels using ant colony algorithm. Composite Structures 2010;92(3):712–719.

[7] Shin DK, Gürdal Z, Griffin Jr OH. Minimum weight design of laminated composite plates for postbuckling performance. Applied Mechanics Reviews 1991;44(11):219–231.

[8] Herencia JE, Weaver PM, Friswell MI. Initial sizing optimisation of anisotropic composite panels with t-shaped stiffeners. Thin-Walled Structures 2008;46(4):399–412.

[9] Bisagni C, Vescovini R. Fast tool for buckling analysis and optimization of stiffened panels. Journal of Aircraft 2009;46(6):2041–2053.

[10] Reddy JN. Mechanics of laminated composite plates and shells: theory and analysis. Boca Raton: CRC Press, 2004.

[11] Weaver PM. Approximate analysis for buckling of compression loaded long rectangular plates with flexural/twist anisotropy. Proceedings of the Royal Society A: Mathematical, Physical and Engineering Science 2006;462(2065):59–73.

[12] Geier B, Meyer-Piening H-R, Zimmermann R. On the influence of laminate stacking on buckling of composite cylindrical shells subjected to axial compression. Composite Structures 2002;55(4):467–474.

[13] Chai GB, Hoon KH. Buckling of generally laminated composite plates. Composite Science and Technology 1992;45(2):125–133.

[14] Romeo G, Frulla G. Analytical/experimental behavior of anisotropic rectangular panels under linearly varying combined loads. AIAA Journal 2001;39(5):932–941.

[15] Shufrin I, Rabinovitch O, Eisenberger M. Buckling of symmetrically laminated rectangular plates with general boundary conditions - a semi analytical approach. Composite Structures 2008;82(4):521–531.

[16] Bisagni C, Vescovini R. Analytical formulation for local buckling and post-buckling analysis of stiffened laminated panels. Thin-Walled Structures 2009;47(3):318–334.

[17] Mittelstedt C, Beerhorst M. Closed-form buckling analysis of compressively loaded composite plates braced by omega-stringers. Composite Structures 2009;88(3):424–435.

[18] Bedair O, Sherbourne A. Unified approach to local stability of plate/stiffener assemblies. Journal of Engineering Mechanics 1995;121(2):214–229.

[19] Wittenberg TC, Hol JMAM, van Baten TJ. Shear buckling of flat orthotropic stiffened panels with application to glare material. AIAA Journal 2006;44(10):2179–2188.

[20] Fujikubo M, Yao T. Elastic local buckling strength of stiffened plate considering plate/stiffener interaction and welding residual stress. Marine Structures 1999;12(9–10):543–564.

[21] Byklum E, Amdahl J. A simplified method for elastic large deflection analysis of plates and stiffened panels due to local buckling. Thin-Walled Structures 2002;40(11):925–953.

[22] Buermann P, Rolfes R, Tessmer J, Schagerl M. A semi-analytical model for local post-buckling analysis of stringer- and frame-stiffened cylindrical panels. Thin-Walled Structures 2006;44(1):102–114.

[23] Vescovini R, Bisagni C. Buckling analysis and optimization of stiffened composite flat and curved panels. AIAA Journal 2012;50(4):904–915.

[24] Nemeth MP. Buckling of long compression-loaded anisotropic plates restrained against inplane lateral and shear deformations. Thin-Walled Structures 2004;42(5):639–685.

[25] Stein M, Neff J. Buckling stresses of simply supported rectangular flat plates in shear. TN 1222, NACA, 1947.

[26] Rastogi N. Buckling of laminated composite plates subjected to combined in-plane bi-axial and shear loads. In: 50^{th} AIAA/ASME/ASCE/AHS/ASC Structures, Structural Dynamics and Material Conference, AIAA-2009-2453, Palm Springs, CA, 4–7 May 2009.

[27] Nemeth MP. Importance of anisotropy on buckling of compression-loaded symmetric composite plates. AIAA Journal 1986;24(11):1831–1835.

[28] Abaqus, version 6.13. User's manual. SIMULIA World Headquarters, Providence, RI, USA, 2013.

[29] Qiao P, Shan L. Explicit local buckling analysis and design of fiber-reinforced plastic composite structural shapes. Composite Structures 2005;70(4):468–483.

[30] Mittelstedt C. Explicit local buckling analysis of stiffened composite plates accounting for periodic boundary conditions and stiffener-plate interaction. Composite Structures 2009;91(3):249–265.

Figure captions

1. Representative unit to describe the behaviour of a larger structure: (a) full model, (b) reduced model accounting for symmetries and anti-symmetries of the buckling modes.

2. Reference system and loading conditions for a generic plate element.

3. Panel dimensions and stiffener foot modeling.

4. Nondimensional buckling load versus aspect ratio for compression loads: (a) panel QI1, (b) panel QI2, (c) panel AP, (d) panel CP.

5. Skin and stiffener local buckling modes of panel AP loaded in compression: (a) $r = 5$ semi-analytical, (b) $r = 5$ Abaqus, (c) $r = 6$ semi-analytical, (d) $r = 6$ - Abaqus.

6. Nondimensional buckling load versus aspect ratio for positive shear loads: (a) panel QI1, (b) panel QI2, (c) panel AP, (d) panel CP.

7. Semi-analytical buckling modes for panel QI1 with aspect ratio $r = 3$: (a) $N_x/N_{xy} = 0.25$, (b) $N_x/N_{xy} = 0.50$, (c) $N_x/N_{xy} = 1.0$, (d) $N_x/N_{xy} = 2.0$.

8. Abaqus buckling modes for panel QI1 with aspect ratio $r = 3$: (a) $N_x/N_{xy} = 0.25$, (b) $N_x/N_{xy} = 0.50$, (c) $N_x/N_{xy} = 1.0$, (d) $N_x/N_{xy} = 2.0$.

9. Interaction curves for biaxial compression: (a) panel QI1, (b) panel QI2, (c) panel AP, (d) panel CP.

10. Interaction curves for combined shear, compression and transverse loads: (a) panel QI1, (b) panel QI2, (c) panel AP, (d) panel CP.

11. Influence of the stiffener foot width on the nondimensional buckling load of panels loaded in compression: (a) panel QI1, (b) panel QI2, (c) panel AP, (d) panel CP.

12. Convergence analysis for panel AP under combined shear and compression, with $N_x/N_{xy} = 0.8$.

Table 1: Feasible buckling mode configurations (S = symmetric, A = anti-symmetric).

Plate element	Mode							
1	S	S	S	S	A	A	A	A
2	A+S	A+S	A+S	A+S	A+S	A+S	A+S	A+S
3	S	S	A	A	S	S	A	A
4	S	A	S	A	S	A	S	A

Table 2: Ply properties.

	E_{11} (MPa)	E_{22} (MPa)	G_{12} (MPa)	ν_{12}	Thickness (mm)
IM7/8552	150000	9000	5300	0.33	0.125

Table 3: Panel lay-ups.

Panel	Skin	Stiffener
QI1	$[\text{-}45°/90°/45°/0°]_s$	[45°/0°/-45°/0°/-45°/0°/45°]
QI2	$[90°/0°/\text{-}45°/45°]_s$	[45°/0°/-45°/0°/-45°/0°/45°]
AP	$[\text{-}45°/45°]_{2s}$	[45°/0°/-45°/0°/-45°/0°/45°]
CP	$[0°/90°]_{2s}$	[0°/90°/0°/90°/0°/90°/0°]

Table 4: Comparison between semi-analytical and numerical results: pure shear, $r = 3$.

	Positive			Negative		
Panel Id	$N_{xy,\text{buck}}$ Analytical (N/mm)	$N_{xy,\text{buck}}$ Abaqus (N/mm)	diff %	$N_{xy,\text{buck}}$ Analytical (N/mm)	$N_{xy,\text{buck}}$ Abaqus (N/mm)	diff %
QI1	22.32	21.60	3.33	12.36	11.80	4.78
QI2	14.78	14.26	3.62	17.11	16.54	3.46
AP	12.52	11.88	5.36	20.01	18.87	6.08
CP	11.68	11.09	5.28	11.68	11.09	5.28

Table 5: Comparison between semi-analytical and numerical results: combined positive shear and compression, $r = 3$.

Panel Id	N_x/N_{xy}	$N_{x,\text{buck}}$ Analytical (N/mm)	$N_{x,\text{buck}}$ Abaqus (N/mm)	diff %
QI1	0.25	4.73	4.57	3.41
	0.50	7.89	7.60	3.91
	1.00	10.88	10.43	4.29
	2.00	11.94	11.35	5.19
QI2	0.25	3.08	3.10	1.05
	0.50	5.18	4.99	3.97
	1.00	7.64	7.32	4.31
	2.00	9.35	8.94	4.60
AP	0.25	2.74	2.60	5.53
	0.50	4.82	4.58	5.23
	1.00	7.56	7.17	5.38
	2.00	10.17	9.63	5.67
CP	0.25	2.54	2.54	0.16
	0.50	4.43	4.23	4.79
	1.00	6.88	6.55	5.04
	2.00	8.72	8.32	4.79

Table 6: Comparison between semi-analytical and numerical results: biaxial loading, $r = 3$.

Panel Id	N_x/N_y	$N_{x,\text{buck}}$ Analytical (N/mm)	$N_{x,\text{buck}}$ Abaqus (N/mm)	diff %
QI1	0.5	3.44	3.32	3.66
	2.0	8.90	8.35	6.62
QI2	0.5	3.88	3.77	2.86
	2.0	8.30	7.83	5.93
AP	0.5	2.57	2.39	7.56
	2.0	8.60	7.90	8.85
CP	0.5	2.79	2.61	6.72
	2.0	6.75	6.38	5.73

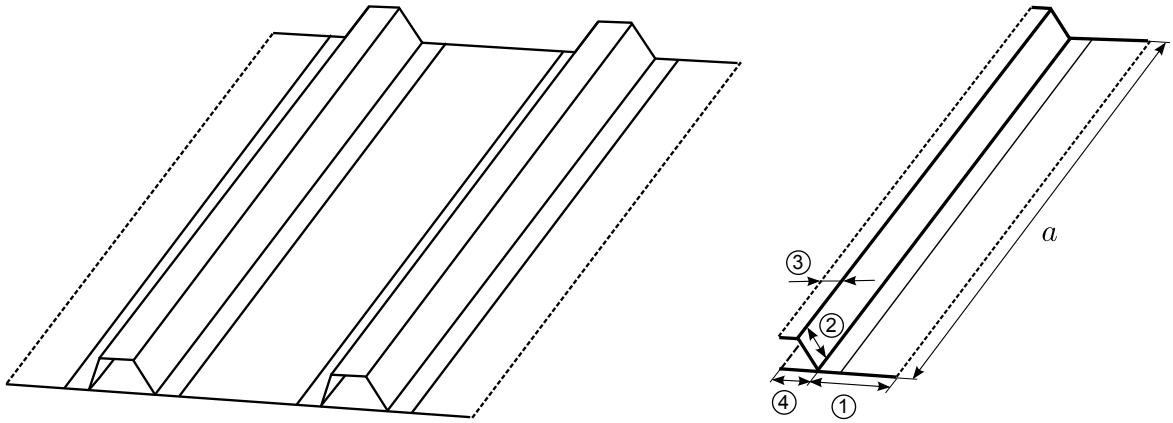

(a) (b)

Figure 1: Representative unit to describe the behaviour of a larger structure: (a) full model, (b) reduced model accounting for symmetries and anti-symmetries of the buckling modes.

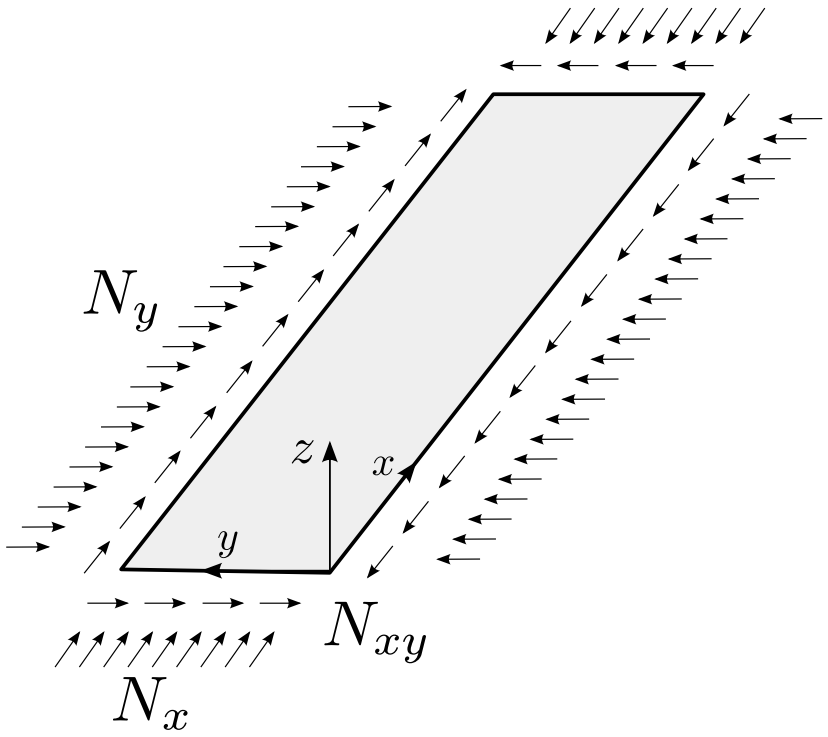

Figure 2: Reference system and loading conditions for a generic plate element.

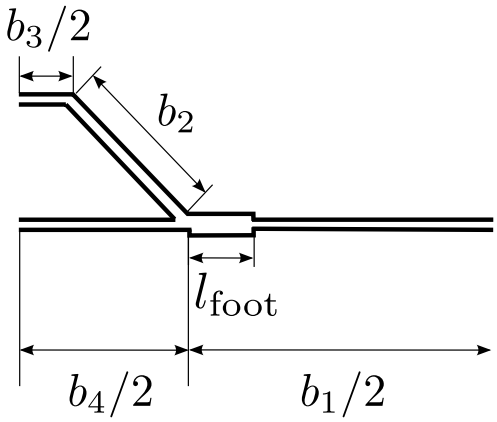

Figure 3: Panel dimensions and stiffener foot modeling.

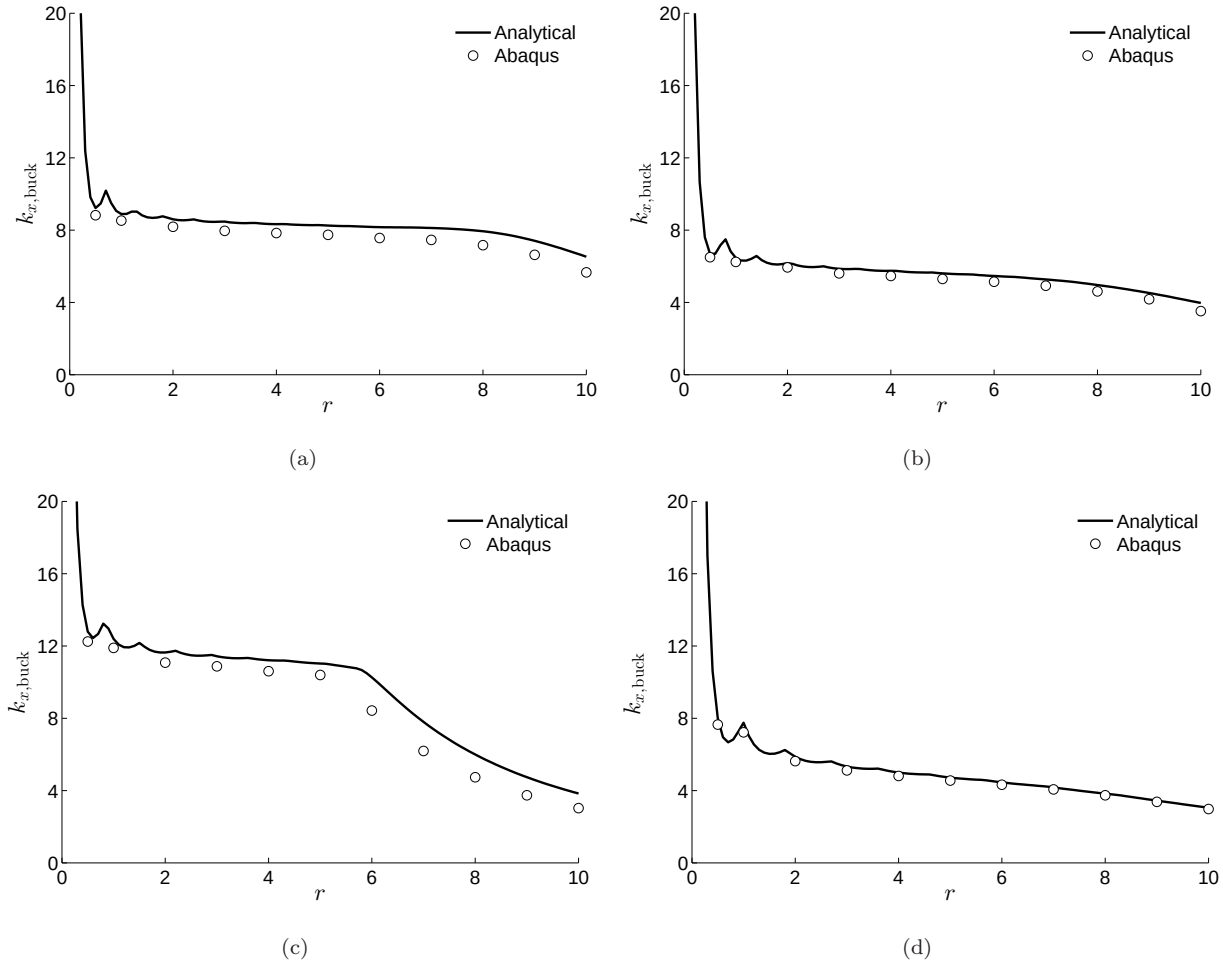

Figure 4: Nondimensional buckling load versus aspect ratio for compression loads: (a) panel QI1, (b) panel QI2, (c) panel AP, (d) panel CP.

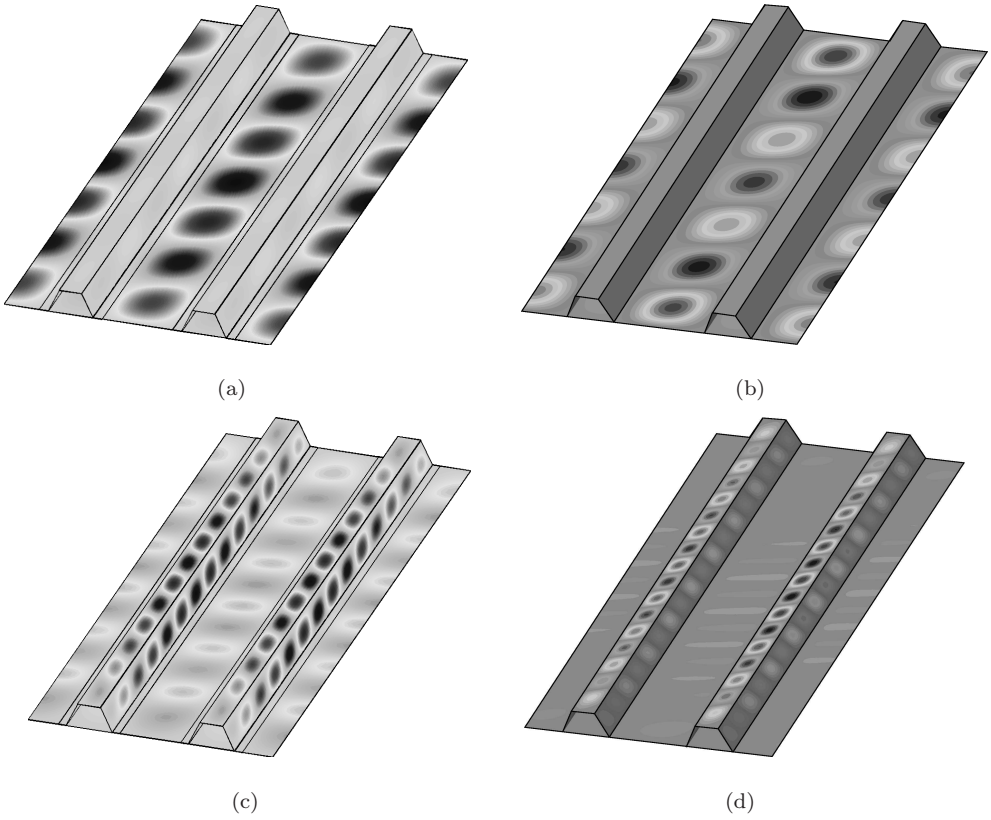

Figure 5: Skin and stiffener local buckling modes of panel AP loaded in compression: (a) $r = 5$ semi-analytical, (b) $r = 5$ Abaqus, (c) $r = 6$ semi-analytical, (d) $r = 6$ - Abaqus.

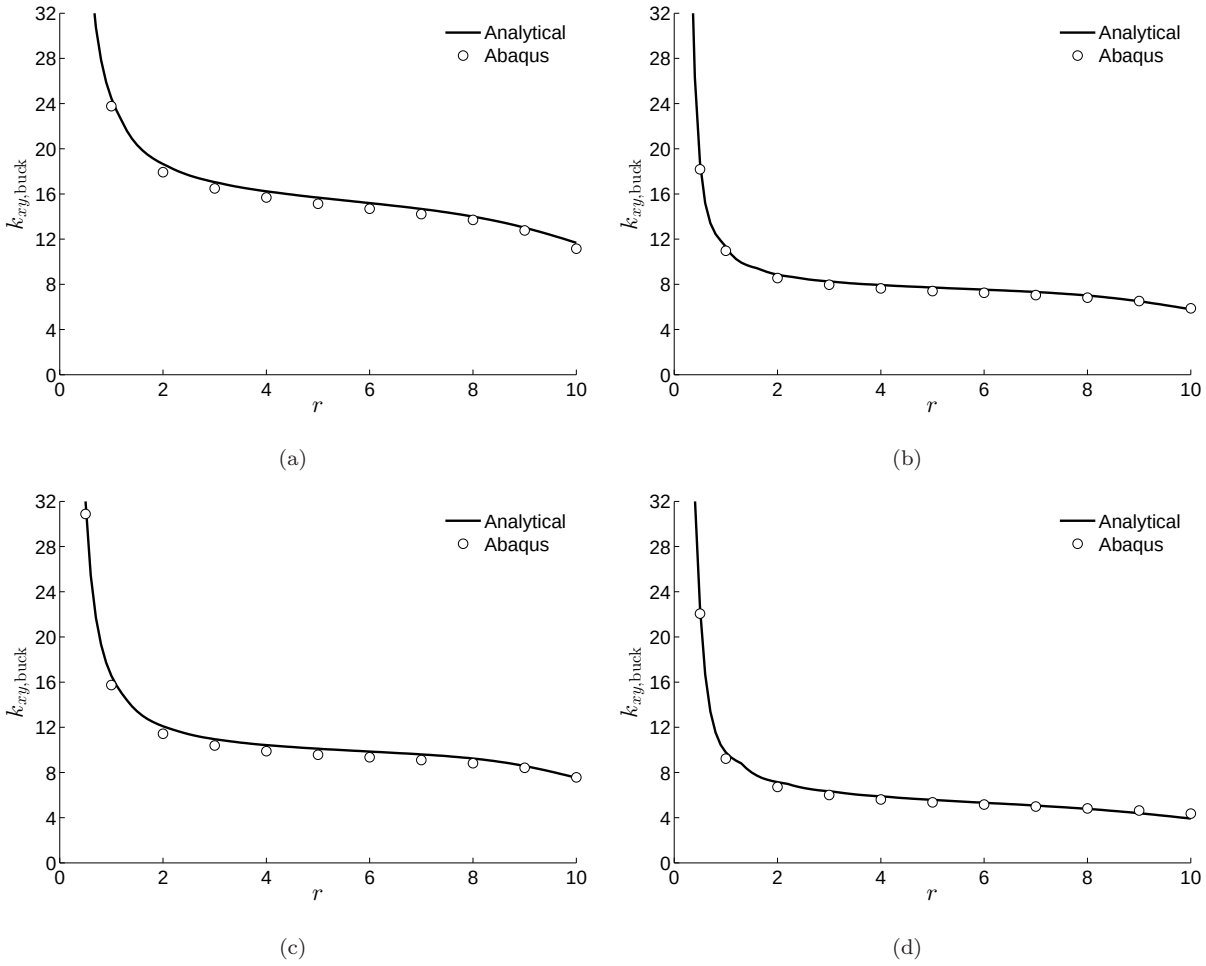

Figure 6: Nondimensional buckling load versus aspect ratio for positive shear loads: (a) panel QI1, (b) panel QI2, (c) panel AP, (d) panel CP.

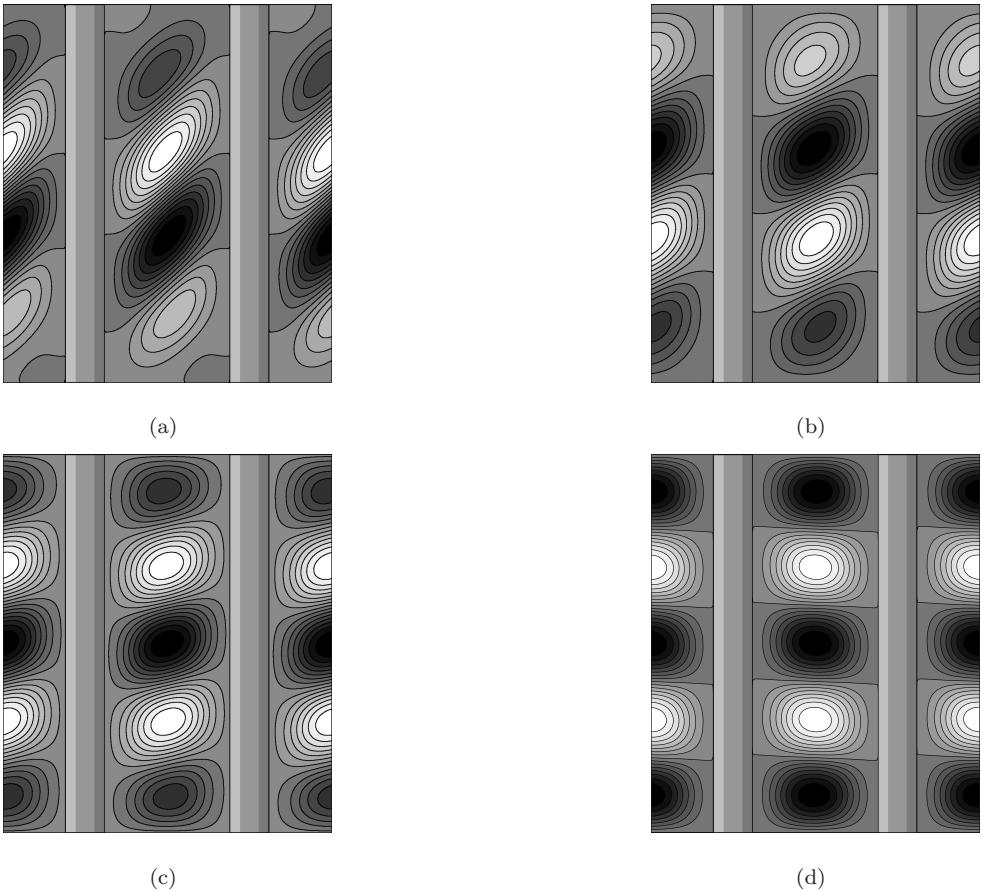

(a) (b)

(c) (d)

Figure 7: Semi-analytical buckling modes for panel QI1 with aspect ratio $r = 3$: (a) $N_x/N_{xy} = 0.25$, (b) $N_x/N_{xy} = 0.50$, (c) $N_x/N_{xy} = 1.0$, (d) $N_x/N_{xy} = 2.0$.

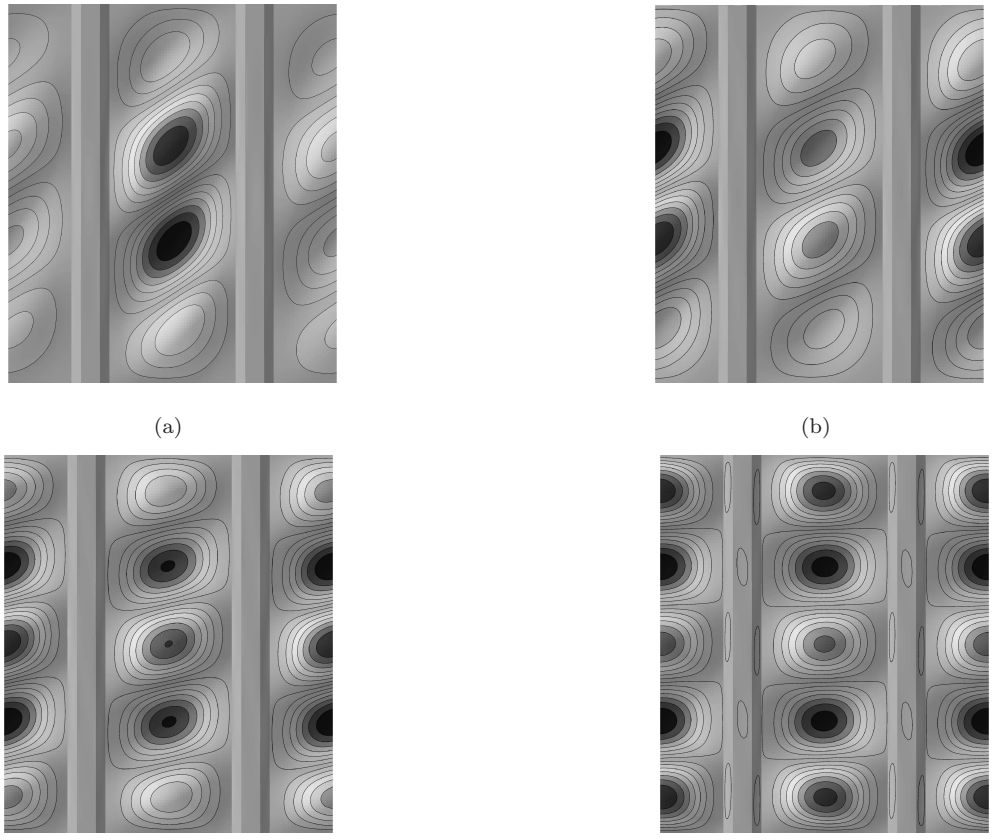

(a) (b)

(c) (d)

Figure 8: Abaqus buckling modes for panel QI1 with aspect ratio $r = 3$: (a) $N_x/N_{xy} = 0.25$, (b) $N_x/N_{xy} = 0.50$, (c) $N_x/N_{xy} = 1.0$, (d) $N_x/N_{xy} = 2.0$.

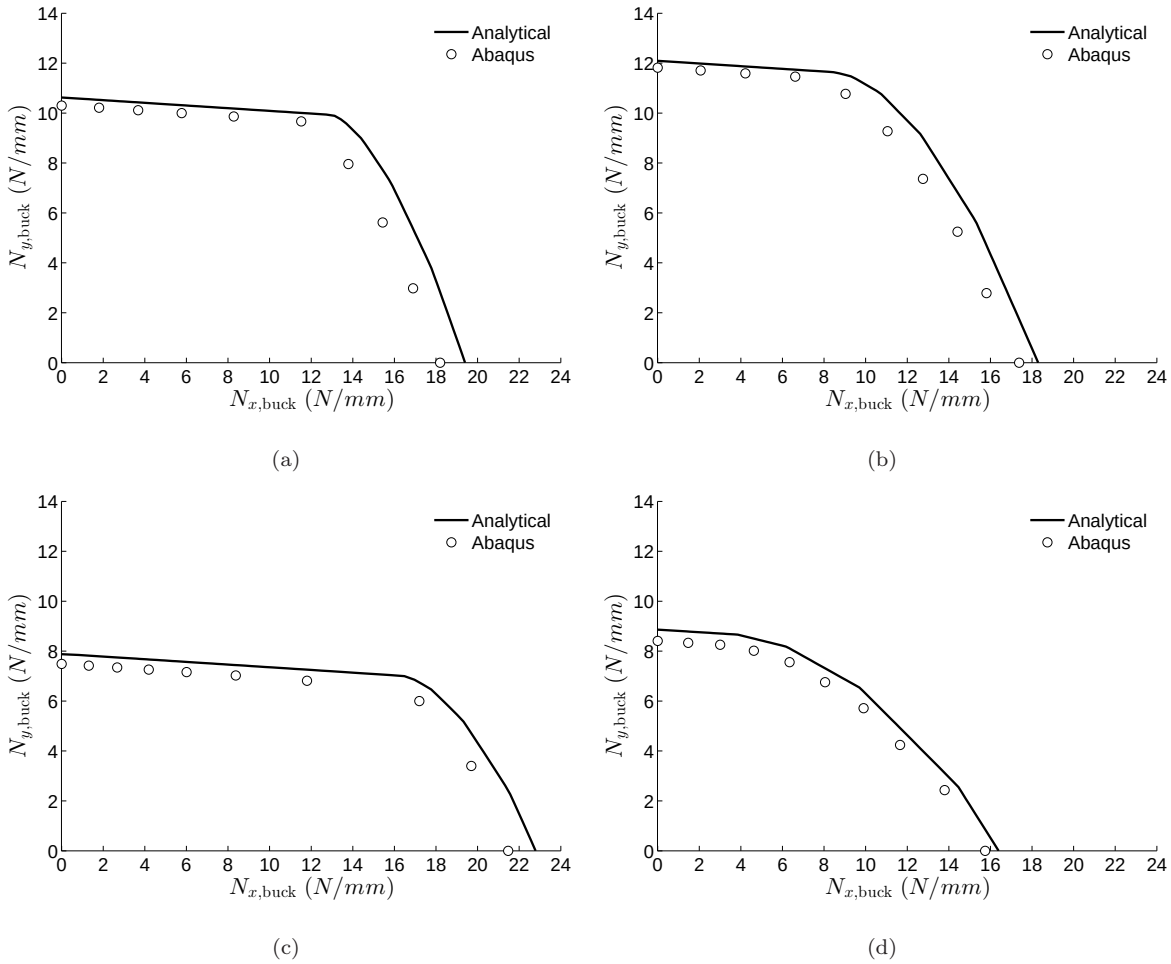

Figure 9: Interaction curves for biaxial compression: (a) panel QI1, (b) panel QI2, (c) panel AP, (d) panel CP.

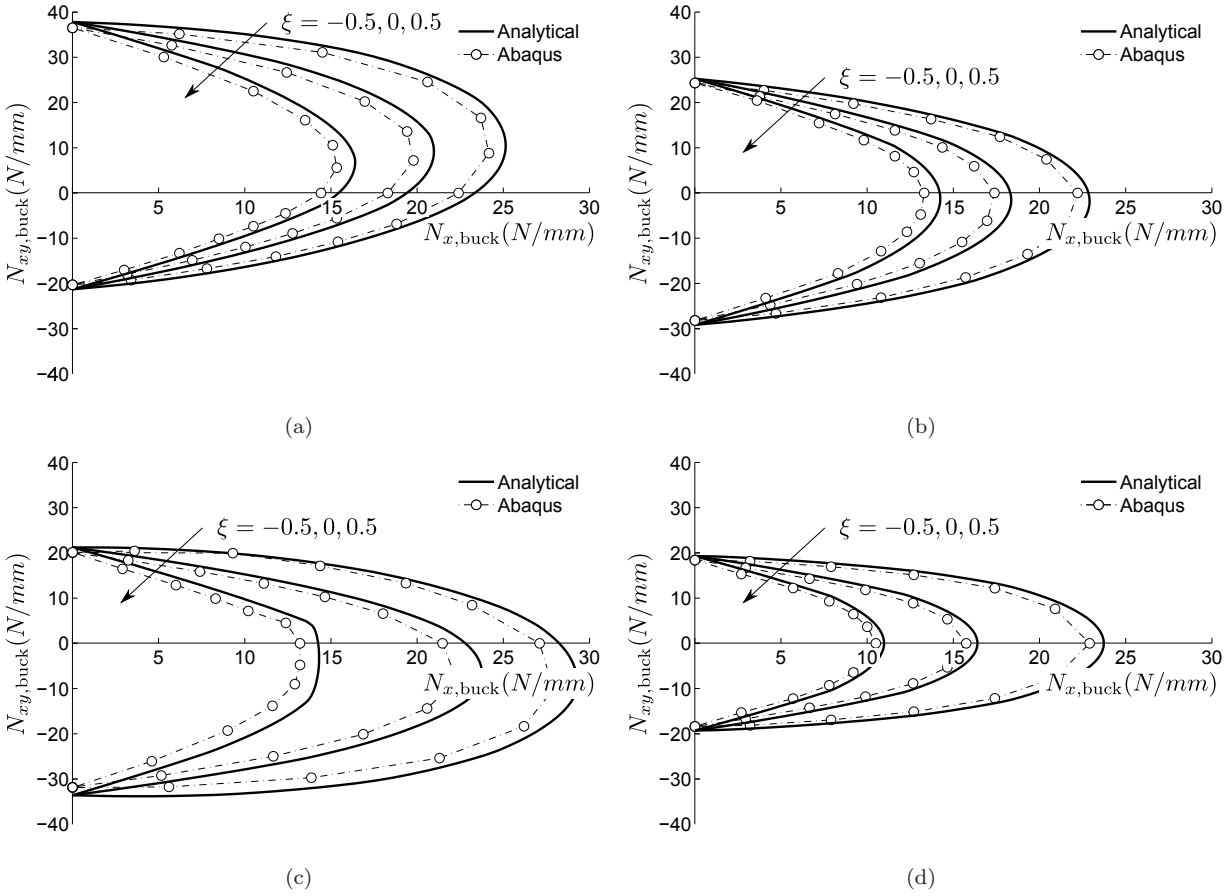

Figure 10: Interaction curves for combined shear, compression and transverse loads: (a) panel QI1, (b) panel QI2, (c) panel AP, (d) panel CP.

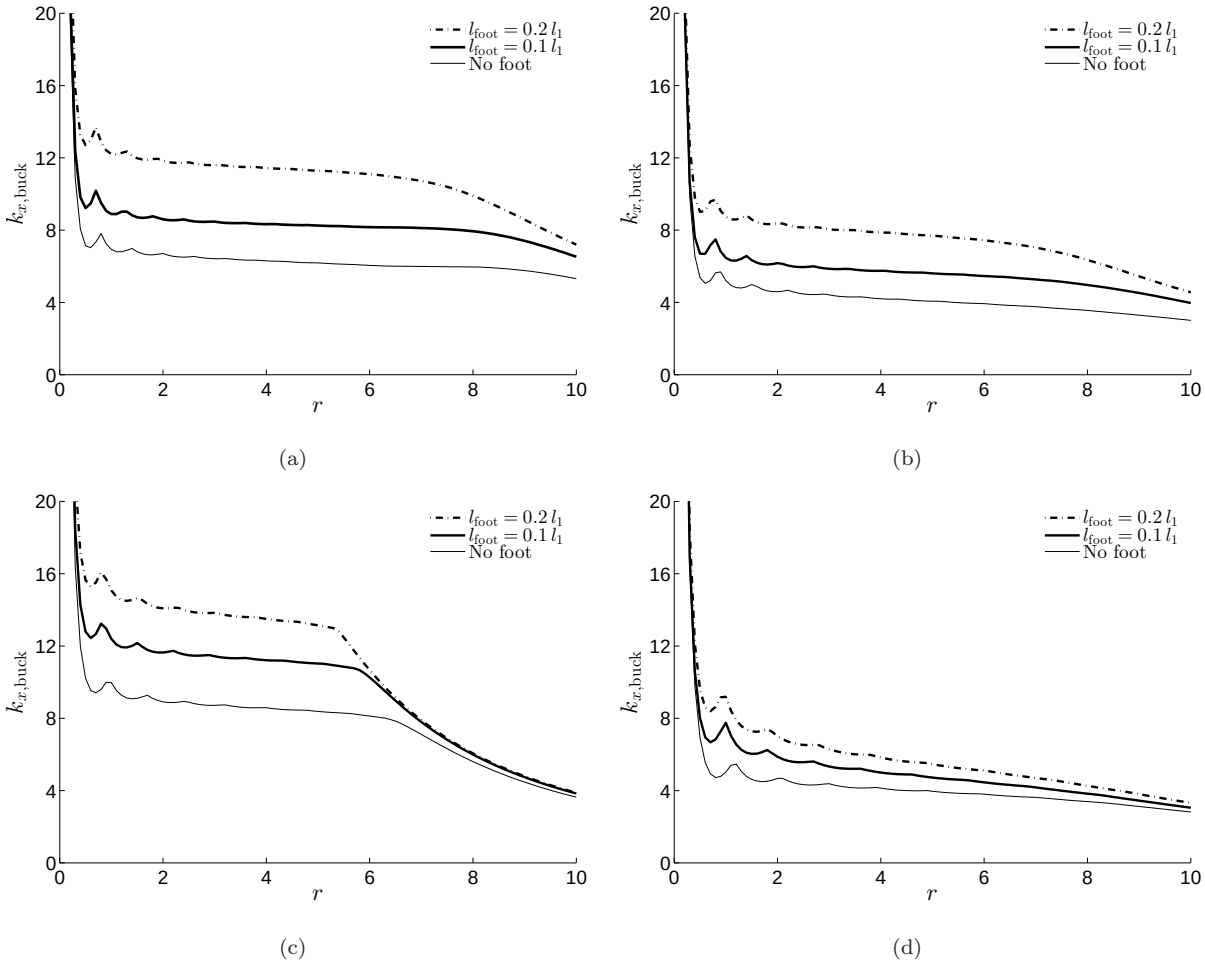

Figure 11: Influence of the stiffener foot width on the nondimensional buckling load of panels loaded in compression: (a) panel QI1, (b) panel QI2, (c) panel AP, (d) panel CP.

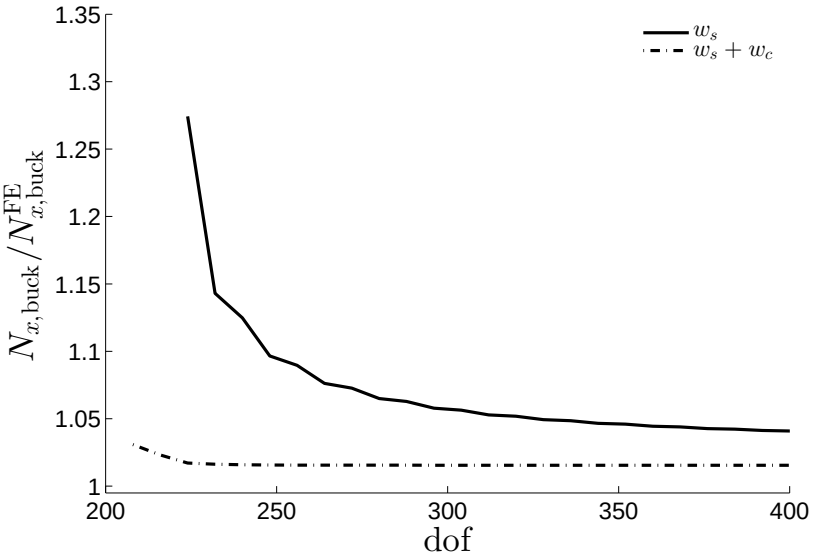

Figure 12: Convergence analysis for panel AP under combined shear and compression, with $N_x/N_{xy} = 0.8$.